

1 1 **Roles of structural defects in polycrystalline platinum nanowires for enhanced**
2 2 **Oxygen Reduction Activity**

3
4 3
5
6 4 Xiao Zhao,^{1,2*} Shinobu Takao,² Yusuke Yoshida,² Takuma Kaneko,² Takao Gunji,²
7 5 Kotaro Higashi,² Tomoya Uruga,^{2,3} and Yasuhiro Iwasawa^{2,4*}

8
9 6 ¹Key Laboratory of Automobile Materials of MOE, School of Materials Science and
10 7 Engineering, Jilin University, Changchun 130012, China

11 8 ²Innovation Research Center for Fuel Cells, The University of
12 9 Electro-Communications, Chofugaoka, Chofu, Tokyo 182-8585, Japan

13 10 ³Japan Synchrotron Radiation Research Institute, SPring-8, Sayo, Hyogo 679-5198,
14 11 Japan

15 12 ⁴Graduate School of Informatics and Engineering, The University of
16 13 Electro-Communications, Chofugaoka, Chofu, Tokyo 182-8585, Japan

17 14 *Corresponding author.

18 15 E-mail address: xzhao417@jlu.edu.cn; iwasawa@pc.uec.ac.jp

19
20
21
22
23
24
25
26
27
28
29
30
31
32
33
34
35
36
37
38
39
40
41
42
43
44
45
46
47
48
49
50
51
52
53
54
55
56
57
58
59
60
61
62
63
64
65

1 **Abstract**

2 Heterogeneous nanocatalysts have uneven surface reactivity and lively change in
3 reactions, making the disclosure of their catalytic origins highly challenging.
4 Phenomenologically, Pt-based nanowires, one of the most important nanostructures,
5 have been noted to display high activity for the oxygen reduction reaction (ORR);
6 however, the fundamentally catalytic origin behind such high performance remains
7 elusive and was implicitly ascribed to one-dimensional structure and/or low-index
8 facets. Here, with molecular-level and operando spectroscopic evidence, we reveal
9 that the polycrystalline platinum nanowires with enhanced ORR activity are closely
10 correlated with structural defects including grain boundaries (GBs) and atomic steps,
11 which is previously neglected or simplified. The local lattice strain is induced by GBs
12 and increases with the misorientation angles of GBs. Despite the same coordination
13 number between edge sites and atomic steps, the latter disturbs interfacial water
14 networks via preferable hydrogen bonding, which destabilizes ORR intermediates on
15 terraces and presumably promotes proton transfer.

16 **Keywords:** oxygen reduction reaction, polycrystalline nanowires, atomic steps, grain
17 boundaries, catalytic defects

1. Introduction

Electrocatalysts are crucial in future energy conversion and storage techniques. In response, rational design of efficient electrocatalysts is indispensable and heavily relies on the knowledge on molecular-level electroactive factors and their operating mechanisms. However, practical nanoelectrocatalysts are structurally heterogeneous at multi-scales, comprise diverse defects and evolve dynamically in reactions, raising forbidden challenges for an in-depth understanding of electrocatalysts. The Pt-based nanocatalysts remain most-efficient for the oxygen reduction reaction (ORR) [1-8], a crucial reaction for fuel cells and metal-air batteries [1-22]. Typically, polycrystalline Pt-based nanowires (PPNWs), one of the most important nanostructures, have been noted to display enhanced ORR activity; however, it is unclear for underlying reasons for activity enhancement. Two general clues, low-index nanofacets [9, 16, 23] and one-dimensional (1D) nanostructure [11, 13] have been proposed. However, some puzzles remain for a long time. At first, PPNWs display an unusual size effect. A much higher ORR activity on 1 nm Pt NWs was reported than on 4.5 nm Pt NWs [9] and 200 nm Pt nanotubes [11, 12] distinct from those nanoparticulate catalysts [24, 25].

More importantly, the roles of defects, like atomic steps and grain boundaries (GBs), are elusive in PPNWs. Reports showed both defect-free PPNWs with Pt (111) facet [11-13] and jagged PPNWs with strained and stepped nanofacets [26] had particularly high ORR performance. Steps binding strongly to ORR intermediates were theoretically speculated inactive or low-active for ORR [25, 27, 28]. However, the acidic ORR activity on high-index facets was reported experimentally higher than on Pt(111) [1]. The GBs, thin interfacial regions between grains, are inherent in polycrystals and proposed to induce catalytically active strained domains [29, 30]. Practical issues remain unanswered regarding how to tune GBs and thus optimize catalytic performance. More importantly, defects are usually reactive and easily reconstructed in reactions, thereby calling for a site-specific and operando understanding of their electrocatalytic behaviors. For example, evidence emerged that

1 surface charging, for example, producing oxygenates on defective or oxophilic sites,
2 brings about the disturbance to interfacial water networks and/or double layer[31-33]
3 and subsequently affect intermediates adsorption[31] and/or mass transport.[32]
4 Recent reports reveal defective or disordered PtNi_x catalysts showed better ORR
5 activity than the common PtNi_x alloy at similar crystalline sizes.[29, 34-37] Despite
6 those important advances, it remains unexplored in details for whether defects in
7 PPNWs play positive roles, and how they operate in ORR.

8 Here, we explored molecular-level electroactive factors resulting in enhanced
9 ORR activity for model PPNWs. Experimental evidence reveals PPNWs's defects
10 comprising atomic steps and GBs benefit ORR. Atomic steps on stepped nanofacets
11 disturb interfacial water networks, destabilizing oxygenates adsorption on terraces.
12 The microstrain is induced by GBs and affected by misorientation angles (MOAs) of
13 GBs, inducing higher ORR activity on more disordered/defective PPNWs. Our
14 insights into molecular-level electroactive factors and their operation mechanisms not
15 only rationalize the enhanced ORR activity on PPNWs but also help design of more
16 efficiency nanoelectrocatalysts, for example, by regulating density, architectures, and
17 interfacial chemistry of GBs.

18 **2. Experimental**

19 **2.1. Materials and Chemicals**

20 Platinum(II) acetylacetonate (Pt(acac)₂), Chloroplatinic acid hexahydrate,
21 cetyltrimethylammonium bromide (CTAB), oleyl amine (OAm), Triton™ X-114,
22 sodium tetrahydridoborate (NaBH₄) and perchloric acid (TraceSELECT) were all
23 purchased from Sigma-Aldrich and used as received without further purification.
24 Ultrapure water (18 MΩ cm) purified in a Millipore system was used in all
25 experiments.

26 **2.2. Preparation of regular PPNWs and PPNWs/C**

27 The synthesis of regular Pt nanowires follows a previous method[14] with a slight
28 modification. Specifically, 20 mg Pt(acac)₂, 50 mg CTAB, and 4 mL OAm were

1 added into 20 mL high pressure vessel. After 30 min ultrasonication of these mixtures,
2 the reaction vessel was dipped into an oil bath pre-heated at 170 °C. After 5 min, 20.3
3 mg Mo(CO)₆ was added into the reaction vessel to reduce Pt(acac)₂ at 170 °C for 2 h.
4 The PPNWs product was precipitated by adding 10 mL ethanol, washed intensively
5 with hexane, and finally dispersed in hexane.

6 Ketjen black carbon was dispersed in 20 ml n-butylamine solvent, to which the
7 regular PPNWs/hexane dispersion was poured, then dispersed thoroughly via
8 ultrasonication, and stirred at room temperature for 24 h to allow for ligand exchange
9 between oleyl amine and n-butylamine. The product was collected by centrifugation
10 and washed with ethanol three times. To ensure complete removal of oleyl amine
11 and/or n-butylamine adsorbed on PPNWs, the catalyst product was heated at 200 °C
12 in air for 1 h in a muffle furnace. The Pt mass percentage was estimated to be 10.0
13 wt% by X-ray fluorescence (XRF).

14 **2.3. Preparation of waved PPNWs and waved PPNWs/C**

15 The synthesis of waved Pt nanowires follows a previous method[38].
16 Specifically, 0.25 mL Triton™ X-114 and 1 mL H₂PtCl₆ solution (15 mg_{Pt}/mL) were
17 added into 50 ml H₂O and intensively stirred for 5 h. Then, 20 mL of freshly prepared
18 NaBH₄ solution (1.5 mg/mL) was poured into the above solution to reduce PtCl₆⁻² and
19 initiate the growth of waved PPNWs. The reaction was continued for 10 min without
20 stirring. The product was collected by centrifugation, washed by ethanol/water
21 solution (V/V=1/1) and finally dispersed in ethanol/water solution.

22 A waved PPNWs solution was poured into 50 ml ethanol/water solution
23 (V/V=1/1) pre-dispersed with Ketjen black carbon. The resultant mixture was stirred
24 for 24 h to allow for the deposition of waved PPNWs on Ketjen black. The catalyst
25 was collected by centrifugation and washed by ethanol/water solution. To remove
26 residual Triton™ X-114 completely, the catalysts-product was heated in air for 2 h.
27 The Pt mass percentage was estimated to be 15.0 wt% by XRF.

28 **2.4. Benchmark Pt/C catalyst**

1 A commercial Pt/C (TEC10E20E) with an average particle size of 2 nm was
2 obtained from Tanaka Kikinzoku Kogyo (TKK) and used as a reference catalyst.
3
4

5 3. Results and discussion

6 3.1. Catalyst characterization and ORR performance

7 We start from two model PPNWs: regular (Figure 1a-d) and waved (Figure 1e-h)
8 PPNWs. Regular PPNWs were synthesized through reducing Pt(acac)₂ by Mo(CO)₆
9 and using cetyltrimethylammonium bromide as a soft template for the PPNWs growth
10 in oleylamine solvent[14] while waved PPNWs via reducing H₂PtCl₆ by NaBH₄ and
11 using Triton™ X-114 as a template in deionized water[38] (see the details in
12 Supporting Information (SI)). The averaged-diameters of regular and waved PPNWs
13 are 1.3±0.3 and 2.2±0.6 nm, respectively (Figure S1). The most notable difference
14 between two PPNWs is in the freedom of grains. Specifically, grains in regular
15 PPNWs are restricted in 1D direction, while in waved PPNWs orientate quite freely in
16 3D directions, consequently appearing more disordered on wave PPNWs (see more in
17 Figures S2-S3).

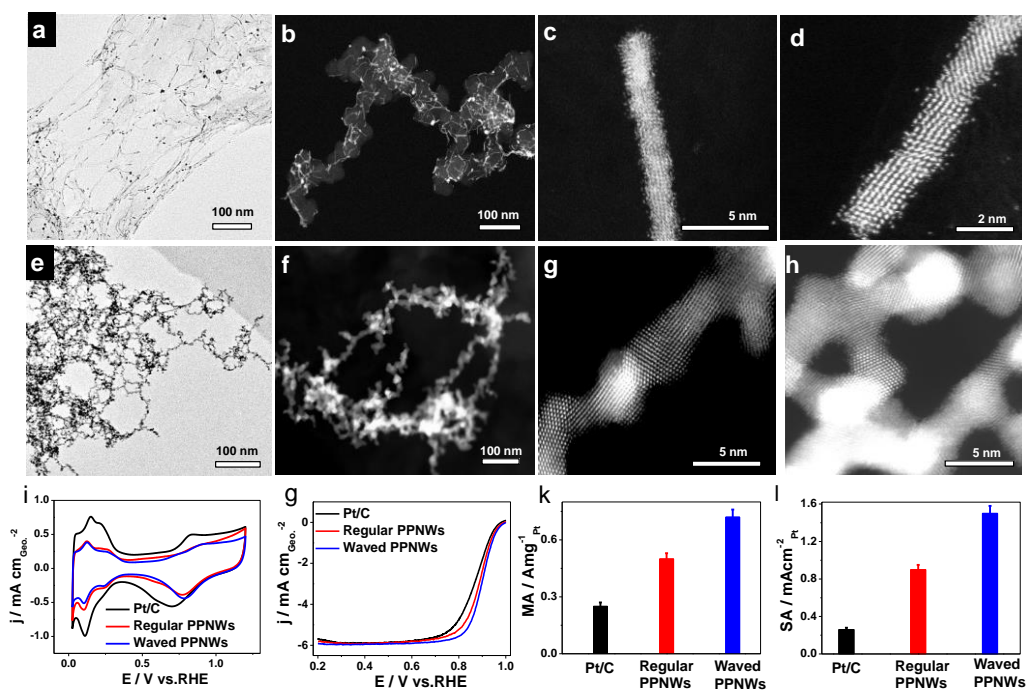
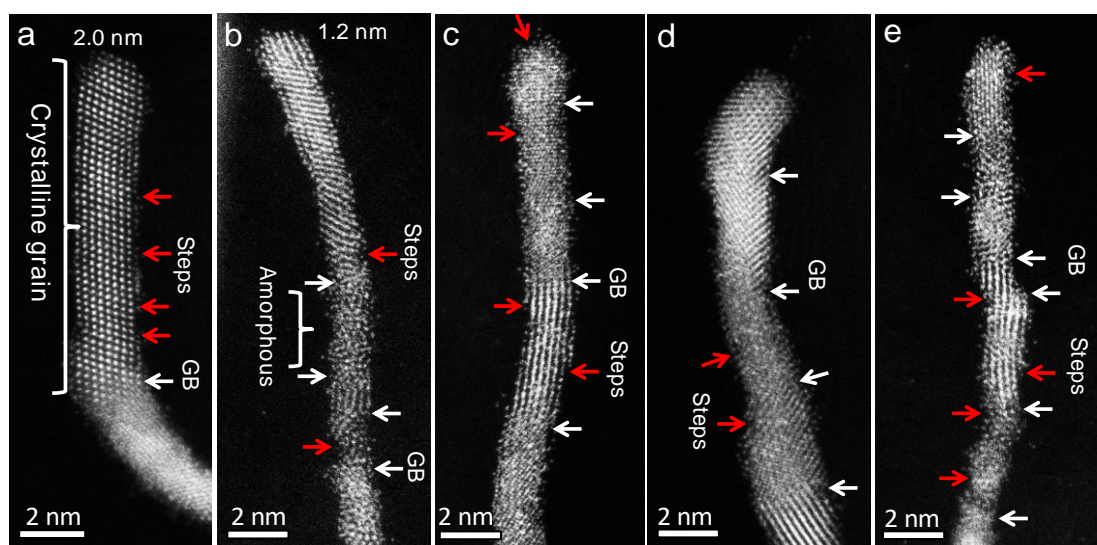


Figure 1: STEM images for (a-d) regular and (e-h) waved PPNWs, as-prepared (a, e) and carbon supported PPNWs (b-d, f-h). (i) Cyclic voltammograms measured in N₂-saturated 0.1 M HClO₄ aqueous electrolyte at 50 mV/s. (g) ORR anodic polarization curves measured at 20 mV/s (1600 rpm). (k-l) Histograms for mass activity (MA, k) and specific activity (SA, l) calculated by Koutecky-Levich equation to obtain mass transport-corrected kinetic current. Pt loadings on three electrodes are 12.0 $\mu\text{gPt cm}^{-2}_{\text{Geo}}$.

We tested ORR performances of carbon-supported regular and waved PPNWs and a benchmark 2.0 nm Pt/C (TEC10E20E). Both regular and waved PPNWs/C display clearly anodically-shifted potentials for *OH/*O desorption and/or surface oxide reduction against 2 nm Pt/C, seen from their cathodic scans in cyclic voltammograms in Figure 1(i). The ORR activities of regular and waved PPNWs/C surpass 2 nm Pt/C regarding Pt-based mass activity (MA, Figure 1(k)) and electrochemical areas-based specific activity (SA, Figure 1(l)). Notably, the SA activity on waved PPNWs/C is higher than on regular PPNWs/C, contrasted with the reports about an improved ORR activity on smaller-sized NWs.[9] [11, 12] Waved PPNWs with a bit larger diameter display a higher activity against regular NWs, indicating a nanostructure-induced enhancement of ORR activity rather than a size effect. Specifically, nanoscale building blocks (i.e. 1-2 nm Pt grains) are similar for

1 the three catalysts; the structural discrepancy accounting for their distinct ORR
2 activities arises from grain organization patterns, i.e. isolated nanoparticles, regular
3 PPNWs, and waved PPNWs. In other words, new structural factors and/or
4 catalytically operating mechanisms are generated to enable enhanced ORR activity for
5 PPNWs.

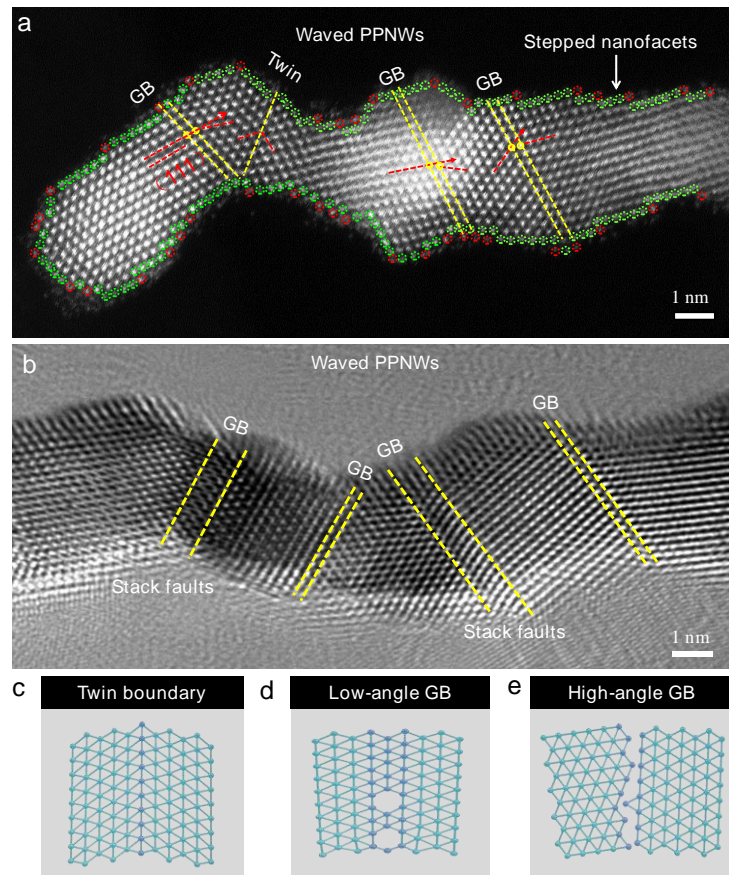
6 3.2. Atomistic analysis of structural defects in PPNWs



7 **Figure 2: Atomistic observation of structural defects and heterogeneities of**
8 **regular PPNWs.** (a-e) HAADF-STEM images. Heterogeneous atomic structures are
9 seen in intra- and inter-NWs, however two general defects, GBs (white arrows) and
10 atomic steps (red arrows), are observable in all measured NWs.

11 An intensive atomistic observation of randomly selected PPNWs demonstrates
12 their polycrystalline nature without any observable single-crystalline NWs (Figure 2,
13 see more in Figure S2). Structural heterogeneity appearing intra-NWs and inter-NWs
14 calls for a sites-specific understanding of their properties. Overall, smaller-diameter
15 PPNWs tend to present a larger defective/disordered degree. For instance, a large
16 domain preferably emerges at 2.0 nm PPNWs (Figure 2a), while an amorphous region
17 arises for 1.2 nm PPNWs (Figure 2b). A thorough examination of all measured
18 PPNWs suggests two general defects: atomic steps and GBs. Notably, most of atomic
19 steps in PPNWs are placed in planes (denoted as the plane-step different from the
20 edge sites of NPs in 2.0 nm Pt/C). We previously presented *in situ* spectroscopic

1 evidence that those plane-steps on stepped nanofacets as templates disturb interfacial
 2 water network and thus destabilize ORR intermediates on vicinal terraces.[31] By
 3 contrast, edge sites over-binding with oxygen contribute negligibly to ORR activity
 4 for Pt NPs.[25, 27, 28] As plane-steps and edge sites have same coordination number
 5 ($CN_{Pt-Pt}=7$), their distinct contributions to ORR activity presumably originate from
 6 different geometry positions. We further through in-situ spectra discuss this point
 7 below.



8

9 **Figure 3: Atomistic observation of stepped nanofacets and GBs of waved PPNWs.**
 10 (a) HAADF-STEM image and (b) high-resolution TEM image for waved PPNWs.
 11 Illustrations of structural models for (c) twin boundary, (d) low-angle GBs, and (e)
 12 high-angle GBs.[39] Red cycles in (a) suggest undercoordinated steps or kinks and
 13 green cycles represent terrace atoms.

14 We further measured atomistic images of waved PPNWs and found the similar
 15 results with regular PPNWs regarding plane-steps and GBs regardless of their varying
 16 nanostructures (Figures 2-3). According to the sizes of misorientation angles (MOAs)

1 and the excessive internal energy, GBs are classified into low-angle GBs (MOAs $<15^\circ$)
2 and high-angle GBs (MOAs $>15^\circ$).[39] The twin is a special boundary between two
3 grains with the relation of mirror reflection. Clearly, the grains in waved PPNWs
4 orientate considerably freely and display large MOAs, resulting in a waved shape
5 against regular PPNWs. Additionally, the stack fault and lattice deformation are
6 observable around GBs (Figures 3 and 4), as GBs could create dislocation pile-ups via
7 hindering dislocation sliding.[39, 40] Expectedly, high-angle GBs with larger MOAs
8 via a dislocation-induced strain field cause more deformed/strained surface atoms[30]
9 that are deviated from the ideal lattice positions and often display unusually catalytic
10 activity. Given this, the overall larger MOAs inducing more catalytically active
11 surface atoms may contribute to a higher ORR activity on waved PPNWs than on
12 regular PPNWs. As the electrocatalyst structure might change dramatically in
13 electrochemical environment and/or during electrolysis, we conducted TEM and
14 HRTEM examination of steps and GBs in PPNWs after the ORR electrocatalysis. The
15 TEM and HRTEM results shown in Figures S6-S7 confirm the absence of dramatic
16 structural change for both regular and waved PPNWs and the still-existing step and
17 GB defects in PPNWs after the ORR electrolysis.

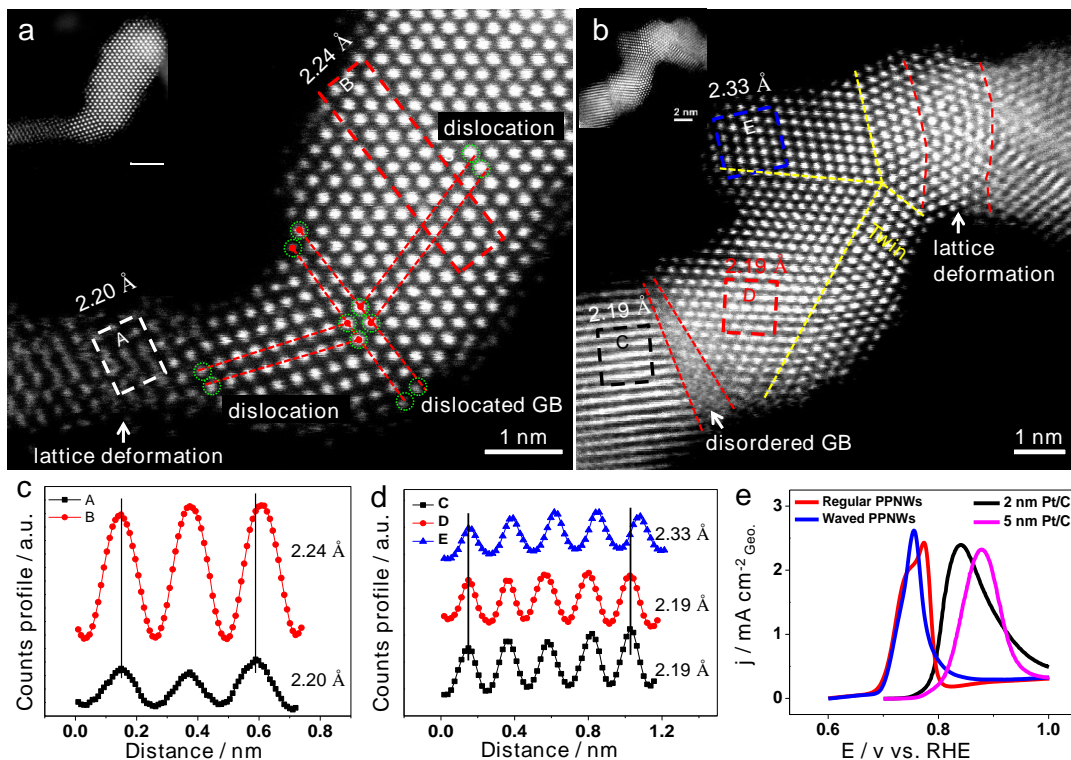


Figure 4: Direct observation of local lattice deformation and dislocations. (a-b)

Atomically-resolved STEM images. (c-d) Inter-planar spacings on selected local lattices. (e) Background-subtracted CO_{ads} stripping voltammograms; Pt loadings for 5 nm Pt/C is 17.8 $\mu\text{g}_{\text{Pt}} \text{cm}^{-2}_{\text{Geo}}$ while for others are 12.0 $\mu\text{g}_{\text{Pt}} \text{cm}^{-2}_{\text{Geo}}$. The red dash lines in (a) indicate the dislocation defects, along which the atoms deviate from the “correct” positions in the crystal structure.

We measured atomic-resolution STEM images to directly present local lattice deformations and dislocations around GBs. At a glance, GBs in PPNWs bring about substantially structural heterogeneities regarding atomic dislocation and lattice distortion. The d spacings of local lattices around GBs (see domains A-E in Figure 4 a-d) vary on a case-by-case basis depending on local micro-environments such as the distances from GBs and edge, MOAs of GBs, and types of GBs (twin, low-angle and high-angle GBs). Of note, the domains A, C, and D appear quite contracted against the bulk Pt (111). Besides, the dislocation-induced microstrain is observable in domains nearby GBs (see the analysis marked by the “dislocation” in Figure 4a). Meanwhile, GBs are a kind of structural defects to accommodate

1 geometrically-misoriented neighboring grains (see Figures 3-4), which could induce
2 microstrain in and around GBs. Together, GBs not only themselves are disordered but
3 also induce strain influence on neighboring grains. Expectedly, GBs and associated
4 lattice microstrains tune d-state of surface Pt atoms and their affinity to reaction
5 intermediates.[41, 42] The STEM presents the definite visual images for the lattice
6 deformation and strain, but they might be a species of the statistically-limited
7 information, which is complemented by the ensemble-level electrochemical and
8 XAFS data.

9 We first estimated samples-averaging defects from a structurally-sensitive *CO
10 stripping reaction.[29, 34, 36] A 5.0 nm Pt/C (TEC10E50E-HT, 50.9 wt.% obtained
11 after a high-temperature heating treatment) was additionally examined for comparison.
12 The kinetics of *CO electrooxidation is known accelerated by crystalline defects like
13 undercoordinated sites via a bifunctional mechanism.[31, 43, 44] A
14 cathodically-shifted *CO stripping peak on 2.0 nm Pt/C against 5 nm Pt/C (see Figure
15 4e) demonstrates the defects active for *CO electrooxidation because 2.0 nm Pt/C has
16 a significantly higher density of undercoordinated sites than 5.0 nm Pt/C.[25]
17 However, both regular and wave PPNWs display enhanced *CO electrooxidation
18 kinetics compared to 2 nm Pt/C, hard to rationalize from the view of the
19 undercoordinated step or edge density. The PPNWs form through an oriented
20 attachment of grains accompanied with disappearance of edges at grain connections.
21 Thereby, a higher step or edge density would not appear in PPNWs than in a
22 similar-size nanoparticulate counterpart. Assuming *CO electrooxidation kinetics
23 were promoted by weakening *CO binding energy, the GBs-induced microstrain (e.g.
24 the compressive lattice microstrain in some deformed domains, see Figure 4 a-b) may
25 facilitate *CO electrooxidation, which was recently suggested by Chattot et al.[29, 34]
26 According to peak potentials of *CO electrooxidation,[29] the defects-induced
27 microstrain follows a decreasing trend: waved PPNWs > regular PPNWs > 2 nm Pt/C.

3.3 In-situ XAFS analysis of structural defects in PPNWs

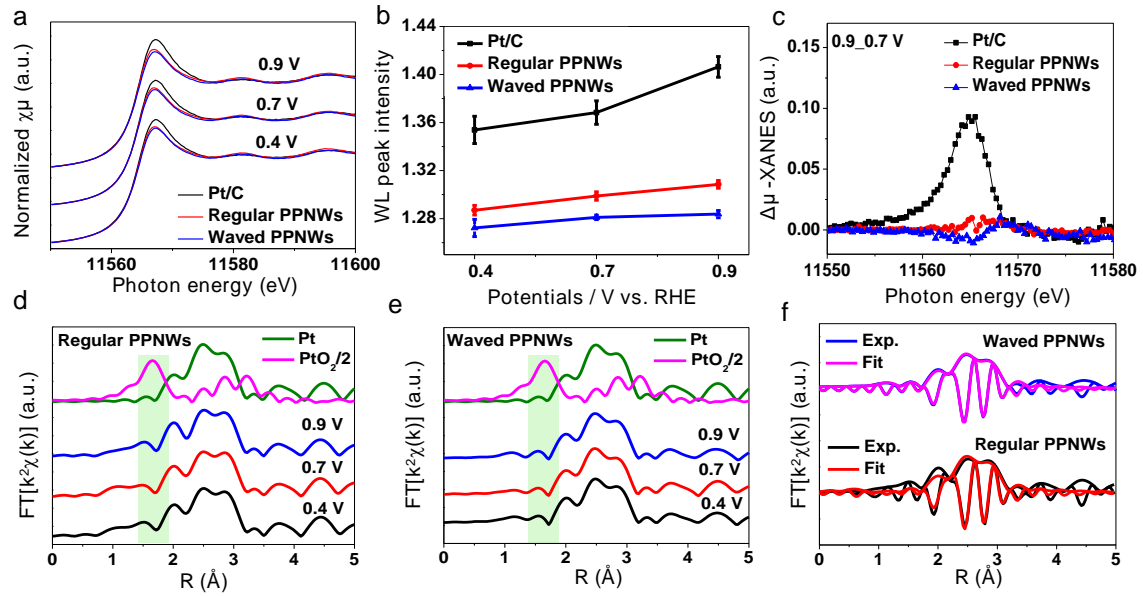


Figure 5: Operando XAFS to trace surface redox and structural parameters under ORR-relevant conditions. (a) XANES of working electrodes and (b) their white-line (WL) peak intensities. (c) $\Delta\mu$ -XANES spectra (0.9 V_0.7 V). (d-e) *In situ* EXAFS Fourier transforms of regular and waved PPNWs show only Pt-Pt scattering peaks when increasing potentials from 0.4 to 0.9 V_{RHE}. (f) Best fits of EXAFS for regular and waved PPNWs at 0.9 V_{RHE} in R space are obtained by only a Pt-Pt scattering shell.

The ORR is a structurally-sensitive reaction. Meanwhile, Pt in ORR experiences the surface redox, associated site-blocking effect and interfacial interaction with adsorbates. These interrelated surface and interfacial processes in turn affect the proceeding of ORR on Pt, making a distinction of structural effects considerably challenging.[45] To this end, we traced Pt surface under ORR-relevant potentials using *in situ* XAFS (Figure 5) in a potential-dependent way. Following by the ORR electrocatalysis, the *in situ* XAFS was measured (see experimental details in SI). For 2 nm Pt/C, the normalized white-line peak intensities of X-ray absorption near edge structure (XANES) at Pt-L₃ edge keep similar when increasing potentials from 0.4 to 0.7 V (vs. RHE) and then increases remarkably from 0.7 to 0.9 V due to the *OH/*O bonding and/or surface oxide generation on Pt surface. By contrast, white-line peak intensities remain almost unchanged from 0.4 to 0.9 V for both regular and waved PPNWs (Figure 5b). Both regular and waved PPNWs appear more metallic (i.e.

1 smaller white line intensity) than 2 nm Pt/C (Figure S4). We further used a $\Delta\mu_{\text{Norm}}$
2 method to reflect the amount and nature of adsorbates on electrodes (Figure 5c). The
3 difference peak areas of $\Delta\mu_{\text{Norm}}(0.9\text{-}0.7\text{V}) = \mu_{\text{Norm}}(0.9\text{ V}) - \mu_{\text{Norm}}(0.7\text{ V})$ decrease in the
4 order: 2 nm Pt/C \gg regular PPNWs \approx waved PPNWs. Particularly, the difference
5 peak intensities of $\Delta\mu_{\text{Norm}}(0.9\text{-}0.7\text{V})$ for regular and waved PPNWs are one order of
6 magnitude smaller than that for 2 nm Pt/C.[31, 46, 47] The *in situ* XANES spectra
7 certify that *OH/*O species electrochemically adsorbed on Pt at 0.9 V are hard to
8 detect by XANES for regular and waved PPNWs, which is entirely different from the
9 case of 2 nm Pt/C. This aspect indicates that those *OH/*O species are quite
10 disordered and thereby their contribution to XANES is weak and even negligible, for
11 which plane-steps can account via their template roles to deform interfacial water
12 networks and bring about a change in interfacial solvation effect relative to Pt
13 (111).[31, 46-48] Consistent with XANES results, the best EXAFS fitting for 2 nm
14 Pt/C needs a Pt-O scattering path due to the presence of discrete surface oxides
15 (Figure S5 and Table S1). By contrast, the *in situ* EXAFS and their curve-fits suggest
16 only a Pt-Pt scattering shell for regular and waved PPNWs (Figure 5d-f). Koper et al.
17 recently demonstrated that adding Ni onto Pt(111) lowers barrier energies of
18 interfacial water reorganization and thus facilitates proton transfer from water to
19 electrodes[32]. Similarly, the proton transfer and oxygen gas transport from
20 electrolyte to electrode in ORR require a significant rearrangement of interfacial
21 water via hydrogen bonds[32, 49]. Given this, the disturbance of plane-steps to
22 interfacial water via their template roles may accelerate proton transfer and
23 consequently benefit proton-coupled electron transfer and ORR[7]. Notably, the edge
24 sites of Pt NPs in 2 nm Pt/C did not result in remarkable disturbance of interfacial
25 water networks, estimated from *in situ* XANES and EXAFS spectra in combination
26 with electrochemical data (Figure 1i). Additionally, edge sites are undercoordinated
27 and their binding to oxygen is too strong to directly electrocatalyze the ORR. Thus,
28 the direct and/or indirect contribution from edge sites is small or negligible for the
29 ORR.

1 As STEM images show different MOAs and associated microstrain between
2 regular and waved PPNWs (Figure 2-4), we further discuss this aspect from the
3 bulk-averaging or ensemble EXAFS. The best fits of EXAFS at 0.4 V (a potential at
4 electric double layer) show that the averaged Pt-Pt interatomic distances ($R_{\text{Pt-Pt}}$) are
5 2.755 ± 0.030 , 2.755 ± 0.009 and 2.758 ± 0.007 Å for 2 nm Pt/C, regular PPNWs, and
6 waved PPNWs, respectively (Table S1-S3). The difference in $R_{\text{Pt-Pt}}$ within fitting error
7 is quite small for the three catalysts and seems hard to interpret their remarkably
8 distinct ORR and *CO electrooxidation activity. Note that the EXAFS-derived $R_{\text{Pt-Pt}}$ is
9 a bulk-averaging value probably masking the local heterogeneity, as shown in STEM
10 images. We thus analyze their structural sources resulting in shortened $R_{\text{Pt-Pt}}$ against
11 bulk Pt (2.775 Å). The $\text{CN}_{\text{Pt-Pt}}$ for 2 nm Pt/C is 8.3 ± 2.1 , which is smaller than $10.7 \pm$
12 2.4 and 11.1 ± 1.0 , respectively for the regular PPNWs and waved PPNWs (Table
13 S1-S3). Undercoordinated surface atoms contract inward[31, 50] either to stabilize the
14 shared electron-pair bonds[51] or to smoothen the surface electronic density, [52, 53]
15 interpreting a shortened $R_{\text{Pt-Pt}}$ for 2 nm Pt/C with a high fraction of uncoordinated
16 surface atoms, like edge and kink sites. However, a little larger $\text{CN}_{\text{Pt-Pt}}$ for the regular
17 and waved PPNWs is expected to result in a bit longer $R_{\text{Pt-Pt}}$, which cannot account
18 for their quite similar $R_{\text{Pt-Pt}}$ and thus suggest new structural sources to induce their
19 shortened $R_{\text{Pt-Pt}}$ rather than the mentioned coordination-dependent surface
20 contraction.[31, 50] On this point, STEM images show direct evidence for the
21 defects-induced microstrain (see Figure 4). This is also supported by the studies of
22 Chattot et al.,[29, 34] who suggested that the structure-sensitive *CO electrooxidation
23 can reflect the trend in lattice microstrain or surface lattice distortion: waved
24 PPNWs > regular PPNWs > 2 nm Pt/C (see Figure 4e). The combined atomistic
25 images, enhanced ORR and *CO electrooxidation activities, and *in situ* XANES and
26 EXAFS spectra suggest that the plane-steps on stepped nanofacets and defect-induced
27 microstrain promote the ORR for the regular and waved PPNWs. Given this, the
28 unusual size effect for PPNWs could be rationalized. For the PPNWs with the same
29 nanostructure, the smaller the grains are, the larger the GBs concentration becomes,

1 thus resulting in a larger fraction of strained surface atoms. In other words, the
2 PPNWs with smaller diameters have more electroactive strained surface atoms that
3 contribute to the enhancement of ORR activity.

4 **4. Conclusion**

5 We explored molecular-level electroactive factors in model PPNWs and
6 revealed the promoting effect of GBs and plane-steps on the acidic ORR. As the local
7 lattice strain increase with the MOAs of GBs, waved PPNWs with larger MOAs
8 showed a better ORR activity than did regular PPNWs. The plane-steps disturbs
9 interfacial water networks via preferable hydrogen bonding, which destabilizes ORR
10 intermediates on terraces and presumably promotes proton transfer; while the
11 edge-sites make almost no positive contribution to ORR activity despite the same
12 coordination number between them. Our experimental results and insights presented
13 here should be valuable for a spectrum of heterogeneous electrocatalytic materials.

15 **Authorship contribution statement**

16 Yasuhiro Iwasawa conceived the research and directed research. Xiao Zhao
17 contributed to experiments and data analysis. Xiao Zhao and Shinobu Takao
18 contributed to the HAADF-STEM analysis. Xiao Zhao, Yusuke Yoshida, Takuma
19 Kaneko, Takao Gunji, Kotaro Higashi, and Tomoya Uruga contributed to the
20 operando XAS analysis. The manuscript was primarily written by Xiao Zhao and
21 Yasuhiro Iwasawa. All authors contributed to discussions and manuscript review.

23 **Declaration of Competing Interest**

24 The authors declare that they have no known competing financial interests or
25 personal relationships that could have appeared to influence the work reported in this
26 paper.

1

2 **Data availability**

3 Data will be made available on request.

5 **Acknowledgement**

6 This work was supported by New Energy and Industrial Technology Development
7 Organization (NEDO), Ministry of Economy, Trade, and Industry (METI), Japan.
8 XAFS measurements were performed with the approval of SPring-8 subject numbers
9 2017A7800, 2017A7801, 2017A7807, 2017A7808, 2017B7800, 2017B7801,
10 2017B7806, 2018A7800, 2018A7801, 2018A7806, 2018B7800, 2018B7801,
11 2019A7800, 2019A7801, 2019B7800, and 2019B7801. STEM measurements were
12 partially conducted under the support of the NIMS microstructural characterization
13 platform through the program "Nanotechnology Platform" of the Ministry of
14 Education, Culture, Sports, Science and Technology (MEXT), Japan. Dr. X. Zhao
15 thanks the support from the startup fund in Jilin University.

16

17 **Appendix A. Supporting information**

18 Supplementary data associated with this article can be found in the online version.

19 **References:**

- 20 [1] L. Zhao, C. Fu, L. Luo, J. You, L. An, X. Yan, S. Shen, J. Zhang, Electrochemical synthesis of
21 monodispersed and highly alloyed PtCo nanoparticles with a remarkable durability towards oxygen
22 reduction reaction, *Appl. Catal., B*, 318 (2022) 121831.
- 23 [2] B.N. Ruggiero, K.M. Sanroman Gutierrez, J.D. George, N.M. Mangan, J.M. Notestein, L.C. Seitz,
24 Probing the relationship between bulk and local environments to understand impacts on
25 electrocatalytic oxygen reduction reaction, *J. Catal.*, 414 (2022) 33-43.
- 26 [3] M. Luo, M.T.M. Koper, A kinetic descriptor for the electrolyte effect on the oxygen reduction
27 kinetics on Pt(111), *Nature Catalysis*, 5 (2022) 615-623.
- 28 [4] J. Huang, L. Sementa, Z. Liu, G. Barcaro, M. Feng, E. Liu, L. Jiao, M. Xu, D. Leshchev, S.-J. Lee, M. Li, C.
29 Wan, E. Zhu, Y. Liu, B. Peng, X. Duan, W.A. Goddard, A. Fortunelli, Q. Jia, Y. Huang, *Experimental*

- 1 Sabatier plot for predictive design of active and stable Pt-alloy oxygen reduction reaction catalysts,
2 Nature Catalysis, 5 (2022) 513-523.
- 3 [5] Q. Cheng, S. Yang, C. Fu, L. Zou, Z. Zou, Z. Jiang, J. Zhang, H. Yang, High-loaded sub-6 nm Pt₁Co₁
4 intermetallic compounds with highly efficient performance expression in PEMFCs, Energy Environ. Sci. ,
5 15 (2022) 278-286.
- 6 [6] C.-L. Yang, L.-N. Wang, P. Yin, J. Liu, M.-X. Chen, Q.-Q. Yan, Z.-S. Wang, S.-L. Xu, S.-Q. Chu, C. Cui, H.
7 Ju, J. Zhu, Y. Lin, J. Shui, H.-W. Liang, Sulfur-anchoring synthesis of platinum intermetallic nanoparticle
8 catalysts for fuel cells, Science, 374 (2021) 459-464.
- 9 [7] T. Wang, Y. Zhang, B. Huang, B. Cai, R.R. Rao, L. Giordano, S.-G. Sun, Y. Shao-Horn, Enhancing
10 oxygen reduction electrocatalysis by tuning interfacial hydrogen bonds, Nature Catalysis, 4 (2021)
11 753-762.
- 12 [8] R. Gao, J. Wang, Z.-F. Huang, R. Zhang, W. Wang, L. Pan, J. Zhang, W. Zhu, X. Zhang, C. Shi, J. Lim,
13 J.-J. Zou, Pt/Fe₂O₃ with Pt-Fe pair sites as a catalyst for oxygen reduction with ultralow Pt loading,
14 Nature Energy, 6 (2021) 614-623.
- 15 [9] K. Jiang, D. Zhao, S. Guo, X. Zhang, X. Zhu, J. Guo, G. Lu, X. Huang, Efficient oxygen reduction
16 catalysis by subnanometer Pt alloy nanowires, Science Advances, 3 (2017) e1601705.
- 17 [10] S. Guo, S. Zhang, D. Su, S. Sun, Seed-Mediated Synthesis of Core/Shell FePtM/FePt (M = Pd, Au)
18 Nanowires and Their Electrocatalysis for Oxygen Reduction Reaction, J. Am. Chem. Soc., 135 (2013)
19 13879-13884.
- 20 [11] C. Koenigsmann, A.C. Santulli, K. Gong, M.B. Vukmirovic, W.-p. Zhou, E. Sutter, S.S. Wong, R.R.
21 Adzic, Enhanced Electrocatalytic Performance of Processed, Ultrathin, Supported Pd-Pt Core-Shell
22 Nanowire Catalysts for the Oxygen Reduction Reaction, J. Am. Chem. Soc., 133 (2011) 9783-9795.
- 23 [12] C. Koenigsmann, W.-p. Zhou, R.R. Adzic, E. Sutter, S.S. Wong, Size-Dependent Enhancement of
24 Electrocatalytic Performance in Relatively Defect-Free, Processed Ultrathin Platinum Nanowires, Nano
25 Lett. , 10 (2010) 2806-2811.
- 26 [13] S.H. Sun, F. Jaouen, J.P. Dodelet, Controlled Growth of Pt Nanowires on Carbon Nanospheres and
27 Their Enhanced Performance as Electrocatalysts in PEM Fuel Cells, Adv. Mater. , 20 (2008) 3900-3904.
- 28 [14] K. Li, X. Li, H. Huang, L. Luo, X. Li, X. Yan, C. Ma, R. Si, J. Yang, J. Zeng, One-Nanometer-Thick
29 PtNiRh Trimetallic Nanowires with Enhanced Oxygen Reduction Electrocatalysis in Acid Media:
30 Integrating Multiple Advantages into One Catalyst, J. Am. Chem. Soc., 140 (2018) 16159-16167.
- 31 [15] H. Liu, W. An, Y. Li, A.I. Frenkel, K. Sasaki, C. Koenigsmann, D. Su, R.M. Anderson, R.M. Crooks, R.R.
32 Adzic, P. Liu, S.S. Wong, In Situ Probing of the Active Site Geometry of Ultrathin Nanowires for the
33 Oxygen Reduction Reaction, J. Am. Chem. Soc., 137 (2015) 12597-12609.
- 34 [16] L. Bu, J. Ding, S. Guo, X. Zhang, D. Su, X. Zhu, J. Yao, J. Guo, G. Lu, X. Huang, A General Method for
35 Multimetallic Platinum Alloy Nanowires as Highly Active and Stable Oxygen Reduction Catalysts, Adv.
36 Mater. , 27 (2015) 7204-7212.
- 37 [17] H. Huang, K. Li, Z. Chen, L. Luo, Y. Gu, D. Zhang, C. Ma, R. Si, J. Yang, Z. Peng, J. Zeng, Achieving
38 Remarkable Activity and Durability towards Oxygen Reduction Reaction Based on Ultrathin Rh-Doped
39 Pt Nanowires, J. Am. Chem. Soc., 139 (2017) 8152-8159.
- 40 [18] Z.W. Chen, M. Waje, W.Z. Li, Y.S. Yan, Supportless Pt and PtPd nanotubes as electrocatalysts for
41 oxygen-reduction reactions, Angew. Chem. Int. Ed., 46 (2007) 4060-4063.
- 42 [19] S.H. Sun, D.Q. Yang, D. Villers, G.X. Zhang, E. Sacher, J.P. Dodelet, Template- and surfactant-free
43 room temperature synthesis of self-assembled 3D Pt nanoflowers from single-crystal nanowires, Adv.
44 Mater. , 20 (2008) 571-574.

- 1 [20] N. Zhang, L. Bu, S. Guo, J. Guo, X. Huang, Screw Thread-Like Platinum–Copper Nanowires
2 Bounded with High-Index Facets for Efficient Electrocatalysis, *Nano Lett.*, 16 (2016) 5037-5043.
- 3 [21] B.Y. Xia, H.B. Wu, N. Li, Y. Yan, X.W. Lou, X. Wang, One-Pot Synthesis of Pt–Co Alloy Nanowire
4 Assemblies with Tunable Composition and Enhanced Electrocatalytic Properties, *Angew. Chem. Int. Ed.*,
5 54 (2015) 3797-3801.
- 6 [22] B.Y. Xia, H.B. Wu, Y. Yan, X.W. Lou, X. Wang, Ultrathin and Ultralong Single-crystal Pt Nanowire
7 Assemblies with Highly Stable Electrocatalytic Activity, *J. Am. Chem. Soc.*, 135 (2013) 9480–9485.
- 8 [23] L. Bu, Y. Feng, J. Yao, S. Guo, J. Guo, X. Huang, Facet and dimensionality control of Pt
9 nanostructures for efficient oxygen reduction and methanol oxidation electrocatalysts, *Nano Research*,
10 9 (2016) 2811-2821.
- 11 [24] M. Nesselberger, S. Ashton, J.C. Meier, I. Katsounaros, K.J.J. Mayrhofer, M. Arenz, The Particle Size
12 Effect on the Oxygen Reduction Reaction Activity of Pt Catalysts: Influence of Electrolyte and Relation
13 to Single Crystal Models, *J. Am. Chem. Soc.*, 133 (2011) 17428-17433.
- 14 [25] M. Shao, A. Peles, K. Shoemaker, Electrocatalysis on Platinum Nanoparticles: Particle Size Effect
15 on Oxygen Reduction Reaction Activity, *Nano Lett.*, 11 (2011) 3714-3719.
- 16 [26] M. Li, Z. Zhao, T. Cheng, A. Fortunelli, C.-Y. Chen, R. Yu, Q. Zhang, L. Gu, B.V. Merinov, Z. Lin, E. Zhu,
17 T. Yu, Q. Jia, J. Guo, L. Zhang, W.A. Goddard, III, Y. Huang, X. Duan, Ultrafine jagged platinum nanowires
18 enable ultrahigh mass activity for the oxygen reduction reaction, *Science*, 354 (2016) 1414-1419.
- 19 [27] A. Kulkarni, S. Siahrostami, A. Patel, J.K. Nørskov, Understanding Catalytic Activity Trends in the
20 Oxygen Reduction Reaction, *Chem. Rev.*, 118 (2018) 2302-2312.
- 21 [28] J.K. Nørskov, J. Rossmeisl, A. Logadottir, L. Lindqvist, J.R. Kitchin, T. Bligaard, H. Jónsson, Origin of
22 the Overpotential for Oxygen Reduction at a Fuel-Cell Cathode, *J. Phys. Chem. B*, 108 (2004)
23 17886-17892.
- 24 [29] R. Chattot, O. Le Bacq, V. Beermann, S. Kühn, J. Herranz, S. Henning, L. Kühn, T. Asset, L. Guétaz, G.
25 Renou, J. Drnec, P. Bordet, A. Pasturel, A. Eychmüller, T.J. Schmidt, P. Strasser, L. Dubau, F. Maillard,
26 Surface distortion as a unifying concept and descriptor in oxygen reduction reaction electrocatalysis,
27 *Nature Mater.*, 17 (2018) 827-833.
- 28 [30] R.G. Mariano, K. McKelvey, H.S. White, M.W. Kanan, Selective increase in CO₂ electroreduction
29 activity at grain-boundary surface terminations, *Science*, 358 (2017) 1187-1192.
- 30 [31] X. Zhao, T. Gunji, T. Kaneko, Y. Yoshida, S. Takao, K. Higashi, T. Uruga, W. He, J. Liu, Z. Zou, An
31 Integrated Single-Electrode Method Reveals the Template Roles of Atomic Steps: Disturb Interfacial
32 Water Networks and Thus Affect the Reactivity of Electrocatalysts, *J. Am. Chem. Soc.*, 141 (2019)
33 8516-8526.
- 34 [32] I. Ledezma-Yanez, W.D.Z. Wallace, P. Sebastián-Pascual, V. Climent, J.M. Feliu, M.T.M. Koper,
35 Interfacial water reorganization as a pH-dependent descriptor of the hydrogen evolution rate on
36 platinum electrodes, *Nature Energy*, 2 (2017) 17031-17037.
- 37 [33] Z. Luo, H. Zhang, Y. Yang, X. Wang, Y. Li, Z. Jin, Z. Jiang, C. Liu, W. Xing, J. Ge, Reactant friendly
38 hydrogen evolution interface based on di-anionic MoS₂ surface, *Nature Communications*, 11 (2020)
39 1116-1124.
- 40 [34] R. Chattot, T. Asset, P. Bordet, J. Drnec, L. Dubau, F. Maillard, Beyond Strain and Ligand Effects:
41 Microstrain-Induced Enhancement of the Oxygen Reduction Reaction Kinetics on Various PtNi/C
42 Nanostructures, *ACS Catal.*, 7 (2017) 398-408.
- 43 [35] X. Zhao, S. Takao, K. Higashi, T. Kaneko, G. Samjeskè, O. Sekizawa, T. Sakata, Y. Yoshida, T. Uruga, Y.
44 Iwasawa, Simultaneous Improvements in Performance and Durability of an Octahedral PtNi_x/C

- 1 Electro catalyst for Next-Generation Fuel Cells by Continuous, Compressive, and Concave Pt Skin Layers,
2 ACS Catal., 7 (2017) 4642-4654.
- 3 [36] R. Chattot, I. Martens, M. Scohy, J. Herranz, J. Drnec, F. Maillard, L. Dubau, Disclosing Pt-Bimetallic
4 Alloy Nanoparticle Surface Lattice Distortion with Electrochemical Probes, ACS Energy Lett., 5 (2020)
5 162-169.
- 6 [37] X. Zhao, S. Takao, T. Kaneko, Y. Iwasawa, Key Factors for Simultaneous Improvements of
7 Performance and Durability of Core-Shell Pt₃Ni/Carbon Electrocatalysts Toward Superior Polymer
8 Electrolyte Fuel Cell, The Chemical Record, 19 (2019) 1337-1353.
- 9 [38] X. Zhao, J. Zhang, L. Wang, H.X. Li, Z. Liu, W. Chen, Ultrathin PtPdCu Nanowires Fused Porous
10 Architecture with 3D Molecular Accessibility: An Active and Durable Platform for Methanol Oxidation,
11 ACS Appl. Mat. Interfaces 7(2015) 26333-26339.
- 12 [39] K. Lu, Stabilizing nanostructures in metals using grain and twin boundary architectures, Nature
13 Reviews Materials, 1 (2016) 16019-16031.
- 14 [40] H. Van Swygenhoven, Grain Boundaries and Dislocations, Science, 296 (2002) 66-67.
- 15 [41] M. Mavrikakis, B. Hammer, J.K. Nørskov, Effect of Strain on the Reactivity of Metal Surfaces, Phys.
16 Rev. Lett. , 81 (1998) 2819-2822.
- 17 [42] M. Gsell, P. Jakob, D. Menzel, Effect of Substrate Strain on Adsorption, Science, 280 (1998)
18 717-720.
- 19 [43] D.S. Strmcnik, D.V. Tripkovic, D. van der Vliet, K.-C. Chang, V. Komanicky, H. You, G. Karapetrov, J.P.
20 Greeley, V.R. Stamenkovic, N.M. Marković, Unique Activity of Platinum Adislands in the CO
21 Electrooxidation Reaction, J. Am. Chem. Soc., 130 (2008) 15332-15339.
- 22 [44] N.P. Lebedeva, M.T.M. Koper, J.M. Feliu, R.A. van Santen, Role of Crystalline Defects in
23 Electrocatalysis: Mechanism and Kinetics of CO Adlayer Oxidation on Stepped Platinum Electrodes, J.
24 Phys. Chem. B, 106 (2002) 12938-12947.
- 25 [45] A.M. Gomez-Marin, R.J. Rizo, J.M. Feliu, Oxygen Reduction Reaction at Pt single crystals: A critical
26 overview, Catalysis Science & Technology, 4 (2014) 1685-1698.
- 27 [46] X. Tian, X. Zhao, Y.-Q. Su, L. Wang, H. Wang, D. Dang, B. Chi, H. Liu, E.J.M. Hensen, X.W. Lou, B.Y.
28 Xia, Engineering bunched Pt-Ni alloy nanocages for efficient oxygen reduction in practical fuel cells,
29 Science, 366 (2019) 850-856.
- 30 [47] Q. Jia, Z. Zhao, L. Cao, J. Li, S. Ghoshal, V. Davies, E. Stavitski, K. Attenkofer, Z. Liu, M. Li, X. Duan, S.
31 Mukerjee, T. Mueller, Y. Huang, Roles of Mo Surface Dopants in Enhancing the ORR Performance of
32 Octahedral PtNi Nanoparticles, Nano Lett. , 18 (2018) 798-804.
- 33 [48] M.J. Kolb, R.G. Farber, J. Derouin, C. Badan, F. Calle-Vallejo, L.B.F. Juurlink, D.R. Killelea, M.T.M.
34 Koper, Double-Stranded Water on Stepped Platinum Surfaces, Phys. Rev. Lett. , 116 (2016)
35 136101-136105.
- 36 [49] T.J.F. Day, U.W. Schmitt, G.A. Voth, The Mechanism of Hydrated Proton Transport in Water, J. Am.
37 Chem. Soc., 122 (2000) 12027-12028.
- 38 [50] W.J. Huang, R. Sun, J. Tao, L.D. Menard, R.G. Nuzzo, J.M. Zuo, Coordination-dependent surface
39 atomic contraction in nanocrystals revealed by coherent diffraction, Nature Mater., 7 (2008) 308-313.
- 40 [51] L. Pauling, Atomic Radii and Interatomic Distances in Metals, J. Am. Chem. Soc., 69 (1947)
41 542-553.
- 42 [52] M.W. Finnis, V. Heine, Theory of lattice contraction at aluminium surfaces, J. Phys. F: Met. Phys. , 4
43 (1974) L37-L41.

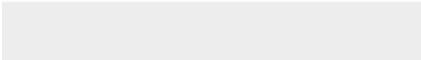
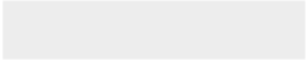
1 [53] R. Smoluchowski, Anisotropy of the Electronic Work Function of Metals, Phys. Rev., 60 (1941)
2 661-674.
3

4
5
6
7
8
9
10
11
12
13
14
15
16
17
18
19
20
21
22
23
24
25
26
27
28
29
30
31
32
33
34
35
36
37
38
39
40
41
42
43
44
45
46
47
48
49
50
51
52
53
54
55
56
57
58
59
60
61
62
63
64
65

- The structural defects in polycrystalline platinum nanowires including grain boundaries and atomic edge-steps benefit oxygen reduction reaction.
- □The grain boundaries induce local lattice strain that depends on misorientation angles.
- □The edge-steps disturb interfacial water networks via preferable hydrogen bonding, which destabilizes oxygenated intermediates on terraces and presumably promotes proton transfer.



Click here to access/download
Supplementary Material
SI-Xiao.pdf



Declaration of interests

The authors declare that they have no known competing financial interests or personal relationships that could have appeared to influence the work reported in this paper.

The authors declare the following financial interests/personal relationships which may be considered as potential competing interests: